ELSEVIER

Journal of Structural Geology 27 (2005) 249–264

JOURNAL OF STRUCTURAL GEOLOGY

www.elsevier.com/locate/jsg

Sense and non-sense of shear in flanking structures with layer-parallel shortening: implications for fault-related folds

Gerhard Wiesmayr*, Bernhard Grasemann

Institut für Geologische Wissenschaften, University of Vienna, A-1090 Vienna, Austria

Received 22 December 2003; received in revised form 2 September 2004; accepted 6 September 2004

Abstract

We investigated the effects of fault-related folding mechanisms along a single fault that is pinned on both ends, upsection and downsection. Using a numerical model we produced *flanking structures* under plane strain transtension for the whole range between simple shear, general shear and pure shear, with layer-parallel shortening parallel and shear zone widening normal to the shear zone boundaries. Under these boundary conditions, contractional flanking folds with thrusting kinematics are the structures that are most likely to form and s-type flanking folds develop stable orientations. Comparison with natural examples reveals that contractional flanking structures occur from the outcrop scale within ductile shear zones, where they can be used as kinematic indicators in special cases, up to the mesoscopic scale within fold and thrust belts. The fundamental differences of our model to existing fault-related fold models like fault-propagation folds, fault-bend folds or break-thrust folds are: (1) the fault does not necessarily maintain a stable orientation but may rotate during progressive development; (2) the drag can change from reverse to normal along the fault; (3) the displacement along the fault has its maximum in the centre of the fault and decreases in both directions, downsection and upsection towards fixed fault tips.

Keywords: Numerical modelling; Transtension; Fault-related folds; Flanking structures

1. Introduction

The phenomenon of various types of deflections of a rock fabric near the margin of faults, dikes or veins, which in some cases can form discrete internal slip surfaces within ductile shear zones, has been recently summarized by Passchier (2001), who introduced the term *flanking structure* for the resulting features. Early numerical models (e.g. Grasemann and Stüwe, 2001) investigated mainly simple shear in the formation of flanking structures and associated drag effects and focused on the effects of the rheological relationship between the fault (here called the cross-cutting element, CE) and the surrounding rock fabric (the host element, HE). If the CE has a significantly lower viscosity than the HE, the CE accommodates slip whereby marker horizons are either displaced in the same or opposite direction as the overall sense of shear along the shear zone (Fig. 1), hence they are either co- or counter-shearing to the bulk sense of shear.

Grasemann et al. (2003) concluded that within a regime of thinning general shear flow (type D plane strain transpression of Fossen and Tikoff (1998)) between the end members of simple shear and pure shear, the resulting flanking structures can be classified into *shear bands, a-type flanking folds and s-type flanking folds* (Fig. 1). These results have been confirmed and extended recently for simple shear by analogue experiments from Exner et al. (2004). Their classification is based on the following three criteria: (1) the extensional or contractional offset of central markers, (2) the co- or counter-shearing sense of slip along CEs with respect to the bulk shear sense, and (3) the normal or reverse drag (Hamblin, 1965) of the central markers relative to the shear sense along the CEs, where *normal drag* occurs if the deflection of the marker line is convex in the direction of shear, whereas *reverse drag* is defined as the concave deflection in the direction of shear (Fig. 1).

Note that for the description of flanking structures, no

* Corresponding author. Tel.: +43-1-4277-53475; fax: +43-1-4277-9534

E-mail addresses: Gerhard.Wiesmayr@univie.ac.at (G. Wiesmayr), Bernhard.Grasemann@univie.ac.at (B. Grasemann).

0191-8141/$ - see front matter © 2004 Elsevier Ltd. All rights reserved.
doi:10.1016/j.jsg.2004.09.001

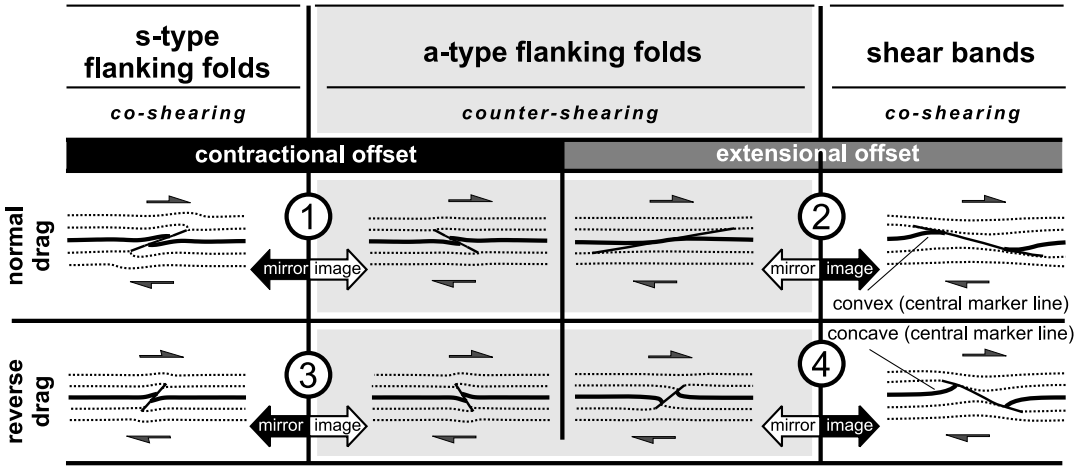

Fig. 1. Four general geometrical types (1–4) of numerically modelled flanking structures in dextral transpression and transtension, all with similar finite bulk strain: s-type, a-type flanking folds and shear bands are distinguished by their contractional vs. extensional offset along the cross-cutting element (CE) and their normal vs. reverse drag of the central marker line. Note that each structure when reflected along a vertical plane exhibits a mirror image of a different type of flanking structure.

unique terminology exists at the moment, as it can either be based on a genetic or purely descriptive (non-genetic) classification. Purely descriptive classifications, like those used by Passchier (2001) and a new one by Coelho et al. (submitted), have the advantage over a genetic one, that they are uniformly applicable in the field without any knowledge of the kinematic frame.

In this article, however, we follow the genetic terminology in order to make our results directly comparable with earlier works (Grasemann and Stüwe, 2001; Grasemann et al., 2003) about flanking structures that have been generated by forward modelling. If the kinematic frame is known, this classification is useful for understanding the progressive evolution of possible geometries even at higher strains (Exner et al., 2004; Kocher and Mancktelow, 2004).

In the present work, we reversed the boundary conditions of Grasemann et al. (2003) of transpressional shear flow and modelled widening shear zones (type D plane strain transtension of Fossen and Tikoff (1998)) covering the whole range between simple shear, general shear and pure shear, in which layer parallel shortening rather than extension takes place parallel to the shear zone boundaries. For the sake of simplicity in this article, we use the terms transtension and transpression for the modelled isochoric plane strain flow, although we are fully aware of the problems of three-dimensional out-of-plane deformation and mixing or confusion of stress and strain related terms (Marrett and Peacock, 1999). We will show that for different kinematic vorticity numbers within plane strain transpression and transtension, four general geometrical types of flanking structures can exist, based on (1) the extensional or contractional offset together with (2) the normal or reverse drag of the central marker (Fig. 1). Although each of these four general types can easily be identified in the field without ancillary information about the bulk shear sense, a corresponding mirror image also exists and therein a problem. To clearly distinguish each structure from its mirror image, additional information (most usually the bulk shear sense of the shear zone) is needed.

Although Grasemann et al. (2003) have already shown that shear bands and a-type flanking folds are ambiguous shear sense indicators, the thrusting kinematics of s-type flanking folds have been regarded as reliable indicators. The data we present reveal that flanking folds formed in such contractional thrusting kinematics can also lead to the wrong shear sense interpretation, if contractional a-type and s-type flanking folds are misinterpreted. Moreover, our results further illustrate that each tectonic regime such as extension or contraction, favours the development of a particular type of flanking structure. Our work thereby shows how flanking structures can be used as an auxiliary tool to distinguish between transpressional and transtensional tectonic settings. Finally, the modelling results presented in this paper are compared with large-scale outcrop natural examples.

A crucial re-assessment that we develop in this article is that, although kinematically completely different, our modelled s-type flanking folds closely resemble fault propagation folds. Using an example from the Himalayas, we suggest that these unrecognised types of fault-related folds may be quite common, and thus extensively misinterpreted in previously studied fold and thrust belts.

2. Numerical modelling

For the investigation of flanking structures forming within a linear viscous medium (HE) around a pinned slip surface (CE) under transtensional flow, as well as for direct comparison with those forming in transpressional flow, we

used the same initial model setup, boundary conditions, and rheology as Grasemann et al. (2003), reversing the applied velocities at the upper and lower boundaries (Fig. 2a). The same two-dimensional finite element program BASIL of Barr and Housemann (1992, 1996) has been used.

2.1. Model setup geometry and boundary conditions

The simulated fault has been modelled as a pinned slip surface (CE) within the central 25% of the total shear zone width and is oriented at a series of increasing fault angles (ϕ10–170°) to the shear zone boundaries (Fig. 2a). The initial model setup geometry that was used is detailed in Grasemann et al. (2003). The length of the shear zone in the spatial x_i-direction is infinite, with faults at equally spaced intervals. The modelled region lies between two of these faults and the distance between them is three times the width of the shear zone in the x_j-direction. For CEs with very shallow fault angles ($\phi = 20°$ and 10°) this distance has been chosen to be four and five times the shear zone width, respectively, to avoid undesirable interferences of neighbouring CEs.

All components of stress and deformation within the shear zone and at the lateral boundaries are continuous, except for the region along the fault, where the shear stress is zero and the normal stress is continuous.

Marker lines within the host element (HE) are oriented parallel to the shear zone boundaries to simulate the fault drag effects on a foliation or layering.

The displacement boundary conditions at the top and bottom of the modelled shear zone are given by the components of the velocity gradient tensor $\boldsymbol{L}$ for

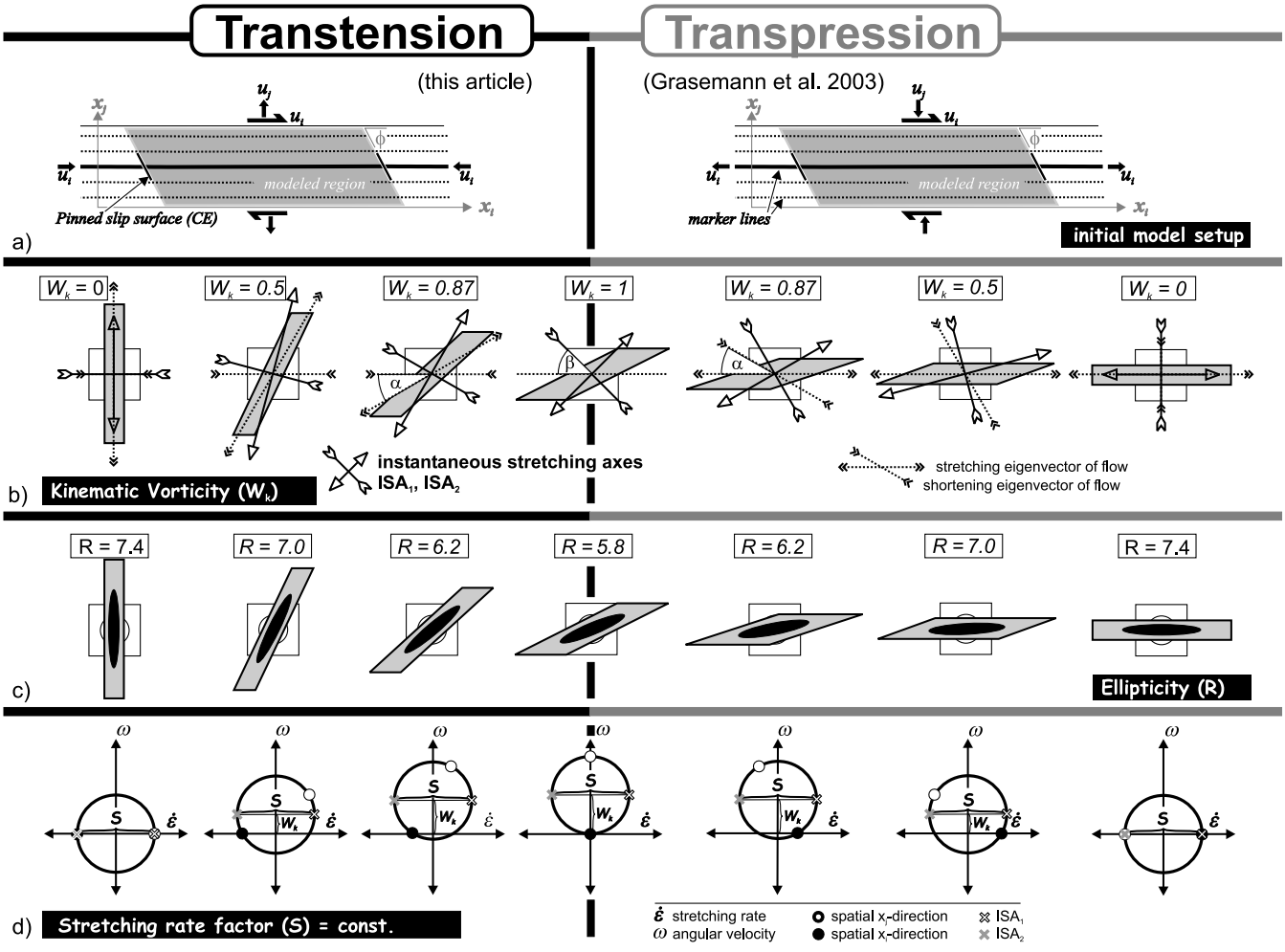

Fig. 2. Illustration of boundary conditions used for numerically modelling transpression and transtension. (a) Initial FEM setup; u_i and u_j are the velocities applied as boundary conditions; ϕ is the fault angle between the CE and the shear zone boundary. (b) Examples of finite deformations of a unit square for various flow types. The stretching (transpression) or the shortening (transtension) eigenvectors are fixed to the x_i-direction. α—angle between eigenvectors, β—angle between the shear zone boundary and ISA_2. (c) Finite strain ellipses resulting from the finite deformations shown in (b). (d) Mohr circle construction illustrating the velocity gradient tensor $\mathbf{L}$ for a constant stretching rate $S = 2$. Instantaneous stretching rates and angular velocities of kinematic axes of the flow are represented as points on the circle.

homogeneous isochoric plane strain flow (Fig. 2a):

$$\boldsymbol{L}_{ij} = \begin{pmatrix} \frac{\partial u_i}{\partial x_i} & \frac{\partial u_i}{\partial x_j} \\ 0 & \frac{\partial u_j}{\partial x_j} \end{pmatrix} \tag{1}$$

where:

$$-\frac{\partial u_i}{\partial x_i} = \frac{\partial u_j}{\partial x_j} \tag{2}$$

In transtensional flow, the shortening eigenvector of the flow is parallel to the shear zone boundaries, whereas in transpressional flow the stretching eigenvector is parallel to these boundaries (Fig. 2b). We assumed steady flow, in which the incremental strain matrix does not change during the deformation history, i.e. the principal instantaneous stretching directions and the kinematic vorticity number W_k remain constant. The flow type is defined by the angle α between the stretching and the shortening eigenvector of the flow and varies between $-90°$ and $0°$ for transtension and between $+90°$ and $0°$ for transpression. As $\cos\alpha = W_k$, the kinematic vorticity number ranges between the ideal end members $W_k = 1$ for simple shear and $W_k = 0$ for pure shear. The angle β defines the orientation of the shortening instantaneous stretching axes (ISA_2) and $\beta + 90°$ is the orientation of the orthogonal instantaneous stretching axes (ISA_1). Along these two axes, minimum and maximum stretching rates of material lines during flow occur. They are related to α by $\beta = (\alpha + 90°)/2$. For the comparison of finite deformation under different flow types, we followed the approach of Grasemann et al. (2003) and used a constant stretching rate factor (Passchier, 1987) of $S = 2$, which is illustrated in Fig. 2d by an off-axis Mohr circle, where the stretching rate ($\dot{\varepsilon}$) is plotted against the angular velocity (ω). If S is constant, all circles have the same diameter and differences in W_k are illustrated by shifting the Mohr circle along the ω-axis, where the distance between the centre of the Mohr circle and the origin defines W_k. The angles measured anticlockwise between the kinematic axes in the physical space in Fig. 2b (instantaneous stretching axes and eigenvectors of the flow) are plotted as points with double angles in a clockwise sense along the Mohr circle.

For a given kinematic vorticity number W_k and a stretching rate factor S, the components of $\boldsymbol{L}$ can be calculated by (modified and corrected after Passchier (1987)):

$$\mathbf{L} = \begin{pmatrix} \frac{S}{2}\sqrt{1 - W_k^2} & W_k S \\ 0 & -\frac{S}{2}\sqrt{1 - W_k^2} \end{pmatrix} \tag{3}$$

The corresponding deformation gradient tensor $\boldsymbol{D}$ given by Ramberg (1975) and combined with Eq. (3) is (corrected after Grasemann et al. (2003)):

$$\boldsymbol{D} = \begin{pmatrix} \exp\left(\frac{St}{2}\sqrt{1 - W_k^2}\right) & \frac{2W_k \sinh\left(\frac{1}{2}St\sqrt{1 - W_k^2}\right)}{\sqrt{1 - W_k^2}} \\ 0 & \exp\left(-\frac{St}{2}\sqrt{1 - W_k^2}\right) \end{pmatrix} \tag{4}$$

where t is the time. For isochoric plane strain flow the components $\boldsymbol{D}_{11}$ and $\boldsymbol{D}_{22}$ of the deformation gradient tensor correspond to the pure shear components k_1 and k_2, respectively, where:

$$\frac{k_1}{k_2} = 1 \tag{5}$$

which means that the volume change during deformation $\Delta V = 0$. $\boldsymbol{D}_{12}$ is the effective shear strain Γ of Fossen and Tikoff (1993). Alternatively, Γ can be calculated from the pure shear component k and W_k using equation (3) of Grasemann et al. (1999). The components of $\boldsymbol{L}$ of the different models, the derived deformation gradient tensor after $t = 1$, and the finite deformation parameters are listed in Table 1. Also note that for a constant stretching rate factor (S) the ellipticity (R) of the finite strain ellipse after the time increment $t = 1$ is not equal for different kinematic vorticities, but varies between $R = 5.8$ and 7.4 between the simple and pure shear end members, respectively (Fig. 2c).

3. Instantaneous structure development

For a series of increasing initial orientation of the CE ($\phi = 10$–$170°$), Fig. 3 shows different diagrams of the instantaneous deflections of the central marker line over a range of pure and simple shear transtension ($\alpha = 0$–$90°$), which can be directly compared with instantaneous deflections in transpression (see fig. 4 of Grasemann et al. (2003)). In each diagram the vertical instantaneous velocity u_j is plotted for each central marker line between two CEs. Different letter codes (C, F, G–J and L–Q) are used to adopt and extend the classification for flanking structures of Grasemann et al. (2003), which is shown in Fig. 4.

Different outlines of the central marker lines in Fig. 3 indicate the sense of rotation of the CE, which can either be co-rotating, counter-rotating or non-rotating with respect to the bulk dextral shear sense of the modelled shear zone. Based on these vertical velocity profiles the following criteria are used for the classification of flanking structures (Fig. 1):

(1) The offset along the CE can be either extensional or contractional.
(2) The sense of shear along the CE can be either co-shearing or counter-shearing compared with the bulk shear sense.
(3) The drag of the central marker line along the CE can be either normal or reverse.

Table 1
List of the deformation parameters used for transtensional finite element models (corresponding parameters for transpression are listed in Grasemann et al., 2003): α—angle between eigenvectors of flow; W_k—kinematic vorticity number; β—angle between ISA_2 and coordinate system: $\beta=(90+\alpha)/2$; S—stretching rate factor; L_{ij}—component of velocity gradient tensor **L** (fig. 2 in Passchier, 1987); D_{ij}—component of rotated general position gradient tensor with $D_{ji}=0$ (Eq. (38) in Ramberg, 1975); $1+e_1$, $1+e_2$—principal strain axes of finite strain ellipsoid; R—ellipticity of finite strain ellipse

α	W_k	β	S	L_{ii}	L_{ij}	L_{ji}	L_{jj}	D_{ii}	D_{ij}	D_{ji}	D_{jj}	$1+e_1$	$1+e_2$	R
−90	0	0	−2	−1	0	0	1	0.367879	0	0	2.718281828	2.718282	0.367879	7.389056
−85	−0.087155743	2.5	−2	−0.996195	0.174311	0	0.996195	0.369282	0.204607603	0	2.707957601	2.715822	0.368213	7.375687
−80	−0.173648178	5	−2	−0.984808	0.347296	0	0.984808	0.373511	0.406219648	0	2.677297133	2.70853	0.369204	7.336133
−75	−0.258819045	7.5	−2	−0.965926	0.517638	0	0.965926	0.380631	0.601971505	0	2.627218879	2.696667	0.370828	7.272015
−70	−0.342020143	10	−2	−0.939693	0.68404	0	0.939693	0.390748	0.789250064	0	2.559194654	2.680656	0.373043	7.185916
−65	−0.422618262	12.5	−2	−0.906308	0.845237	0	0.906308	0.404013	0.965794795	0	2.475166798	2.661056	0.375791	7.081218
−60	−0.5	15	−2	−0.866025	1	0	0.866025	0.420620	1.129772083	0	2.377442675	2.638541	0.378997	6.961901
−55	−0.573576436	17.5	−2	−0.819152	1.147153	0	0.819152	0.440805	1.279818396	0	2.26857537	2.61387	0.382575	6.832315
−50	−0.64278761	20	−2	−0.766044	1.285575	0	0.766044	0.464848	1.415050804	0	2.15124005	2.587849	0.386421	6.696965
−45	−0.707106781	22.5	−2	−0.707107	1.414214	0	0.707107	0.493069	1.53504629	0	2.028114982	2.561309	0.390425	6.560302
−40	−0.766044443	25	−2	−0.642788	1.532089	0	0.642788	0.525825	1.639793734	0	1.901774903	2.535066	0.394467	6.426558
−35	−0.819152044	27.5	−2	−0.573576	1.638304	0	0.573576	0.563506	1.729624314	0	1.774602468	2.509903	0.398422	6.299614
−30	−0.866025404	30	−2	−0.5	1.732051	0	0.5	0.606531	1.805127089	0	1.648721271	2.486546	0.402164	6.182909
−25	−0.906307787	32.5	−2	−0.422618	1.812616	0	0.422618	0.655329	1.86705688	0	1.525951671	2.465643	0.405574	6.079396
−20	−0.939692621	35	−2	−0.34202	1.879385	0	0.34202	0.710334	1.916241201	0	1.407788655	2.447758	0.408537	5.991521
−15	−0.965925826	37.5	−2	−0.258819	1.931852	0	0.258819	0.771963	1.953492262	0	1.295399375	2.433359	0.410955	5.921234
−10	−0.984807753	40	−2	−0.173648	1.969616	0	0.173648	0.840593	1.97952897	0	1.189636951	2.42281	0.412744	5.870009
−5	−0.996194698	42.5	−2	−0.087156	1.992389	0	0.087156	0.916534	1.99491276	0	1.091066592	2.416376	0.413843	5.838872
0	−1	45	−2	0	2	0	0	1.000000	2	0	1	2.414214	0.414214	5.828427

Based on these three criteria, Fig. 4 gives a detailed overview of the instantaneous structural development for the full range of possible initial fault angles ϕ calculated in 10° steps. For the whole range of transpression and transtension, three types of instantaneously developing flanking structures can be distinguished, and these are presented in three major fields in Fig. 4. These types are: (1) s-type flanking folds, which reveal contractional offset and are co-shearing, (2) a-type flanking folds, which can have both contractional or extensional offset, but they are counter-shearing, and (3) shear bands, which reveal an extensional offset and are co-shearing.

The fields are subdivided by the non-shearing, oblique instantaneous stretching axes (ISA_1 and ISA_2) where the shear sense changes from co-shearing to counter-shearing along ISA_2 (i.e. from shear bands to a-type flanking folds) and from counter-shearing back to co-shearing along ISA_1 (i.e. from a-type flanking folds to s-type flanking folds). All three types can either develop with a normal or reverse drag effect. While a-type flanking folds always co-rotate during progressive deformation, s-type flanking folds and shear bands can either co- or counter-rotate. Correspondingly, these fields can be subdivided along lines where no rotation occurs and structures become stable or metastable.

If the CE is oriented at a low angle ($\phi = 0$–$25°$) or high angle ($\phi = 155$–$180°$) with respect to the shear zone boundary, flanking structures develop a normal drag effect, irrespective of the flow type (Fig. 4).

3.1. Co-shearing, counter-shearing and non-shearing structures

Structures Ga and Gb do not develop any offset and any drag instantaneously, as they have the same orientation as the non-shearing ISA_2 and ISA_1, respectively. Consequently, they mark the boundary between co-shearing structures, i.e. shear bands and s-type flanking folds, and counter-shearing structures, i.e. a-type flanking folds.

3.2. Co-rotating or counter-rotating structures

Assuming a constant W_k, the change in orientation and the sense of rotation of the CE during progressive deformation can be determined when following vertical lines from the point representing the initial orientation in the diagram (Fig. 4). For example the CE of structures Ga and Gb will, therefore, in almost all cases (except the transpressional pure shear end member Ga) rotate towards higher angles ϕ during progressive deformation as they plot in the field of co-rotation. Structures Ga will develop into a-type flanking folds, which are always co-rotating. Depending on the flow type and the angle ϕ, structures H–K will develop. Structures Gb will develop into s-type flanking folds (structures L, M and O). Similar to the results for shear bands (Grasemann et al., 2003), s-type flanking folds can either co- or counter-rotate depending on W_k and the initial orientation of the CE. For the case of pure shear ($W_k = 0$), s-type flanking folds and shear bands will always counter-rotate irrespective of the angle ϕ, which can range between $\phi = 0$–$90°$ for shear bands and $\phi = 90$–$180°$ for s-type flanking folds. With increasing W_k, the probability of counter-rotation of the CE decreases (i.e. structures A and D for shear bands and structures N and Q for s-type flanking folds). Remaining shear band types will always be co-rotating, in which case the probability of shear band development (structures C and F) progressively decreases away from the transpressional pure shear end member and is limited to small angles $\phi \sim 10$–$30°$ in transtension. At the same time the probability of co-rotating s-type flanking fold development (structures L and O) progressively decreases away from the transtensional pure shear end member and is limited to high angles $\phi \sim 150$–$170°$ in transpression.

3.3. Non rotating and stable-metastable CE orientations

Only in the case of the transpressional pure shear end member Ga does a metastable structure form, and this can either develop into a reverse drag shear band or an extensional a-type flanking fold (Fig. 4). Gb on the transtensional pure shear side remains stable.

Structures that form in the area on the graph in Fig. 4 marked by thick black bold and dashed lines will develop into stable and metastable structures, respectively, as the CE is not rotating.

For stable structures (structures B, Gb and M), a deviation from the non-rotating orientation of the CE results in an immediate co- or counter-rotation back into the original non-rotating position. This is the case where arrowheads in Fig. 4 are pointing in opposing directions towards the stable structure. For metastable structures (structures E, Ga and P), however, a slight deviation of ϕ

Fig. 3. Calculated deformation of the central marker line, where the vertical instantaneous velocity u_j is plotted for the length of the central marker line between two repeating CE, for different flow types of dextral transtension (see Grasemann et al. (2003) for dextral transpression). The fault angle varies between $\phi = 10°$ and 170° ((a)–(q)). α is the angle between the eigenvectors of the flow, where $\alpha = 0°$ for simple shear and $\alpha = 90°$ for pure shear. The marker lines are labelled with letter codes corresponding to the instantaneous flanking structures classified in Fig. 4. Different line patterns are used for co-, non- and counter-rotating CEs. Thick dotted lines show orientations of CEs that are parallel to either ISA_2 or ISA_1.

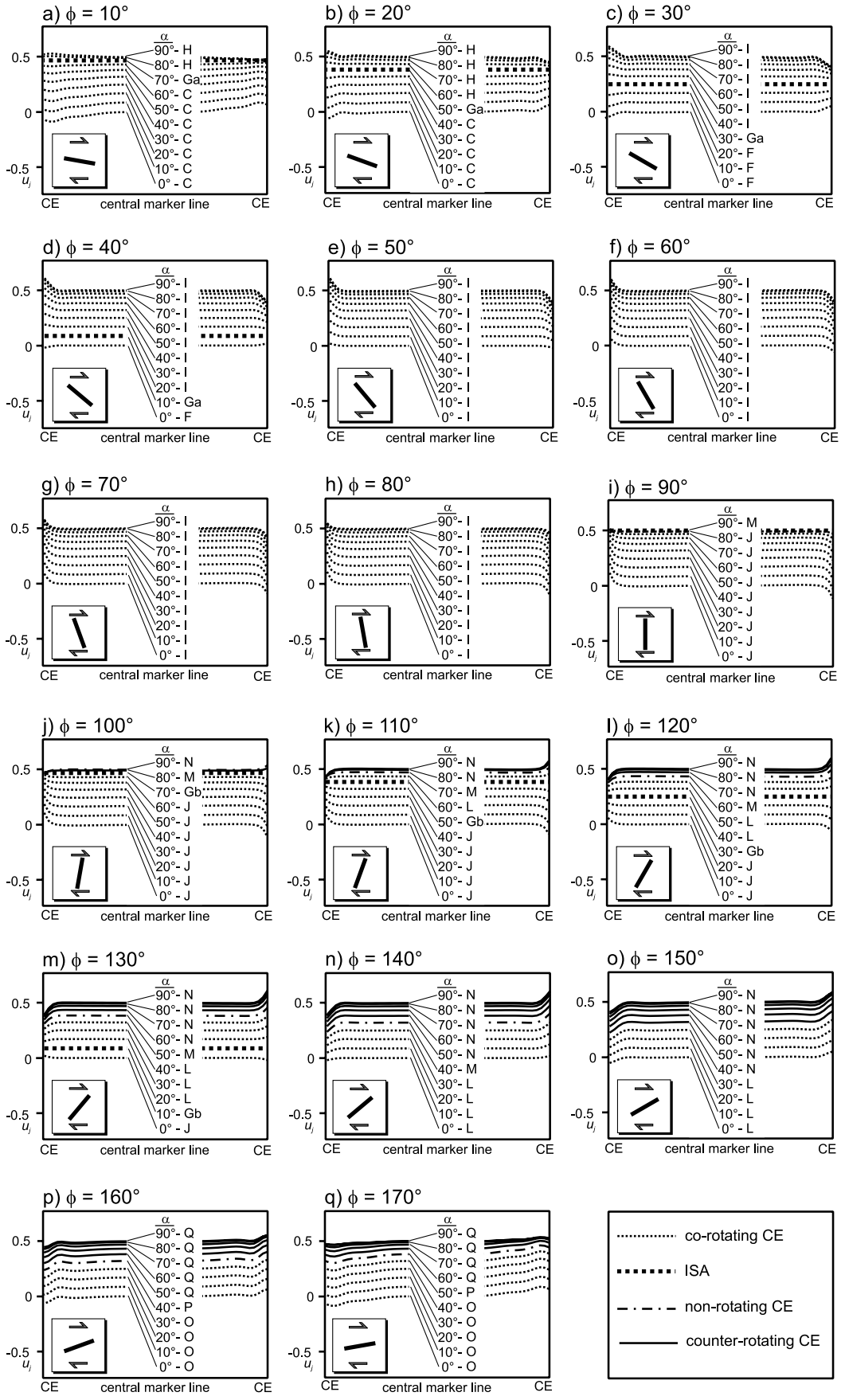
a) ϕ = 10°
α
90°- H
80°- H
70°- Ga
60°- C
50°- C
40°- C
30°- C
20°- C
10°- C
0° - C
b) ϕ = 20°
α
90°- H
80°- H
70°- H
60°- H
50°- Ga
40°- C
30°- C
20°- C
10°- C
0° - C
c) ϕ = 30°
α
90°- I
80°- I
70°- I
60°- I
50°- I
40°- I
30°- Ga
20°- F
10°- F
0° - F
d) ϕ = 40°
α
90°- I
80°- I
70°- I
60°- I
50°- I
40°- I
30°- I
20°- I
10°- Ga
0° - F
e) ϕ = 50°
α
90°- I
80°- I
70°- I
60°- I
50°- I
40°- I
30°- I
20°- I
10°- I
0° - I
f) ϕ = 60°
α
90°- I
80°- I
70°- I
60°- I
50°- I
40°- I
30°- I
20°- I
10°- I
0° - I
g) ϕ = 70°
α
90°- I
80°- I
70°- I
60°- I
50°- I
40°- I
30°- I
20°- I
10°- I
0° - I
h) ϕ = 80°
α
90°- I
80°- I
70°- I
60°- I
50°- I
40°- I
30°- I
20°- I
10°- I
0° - I
i) ϕ = 90°
α
90°- M
80°- J
70°- J
60°- J
50°- J
40°- J
30°- J
20°- J
10°- J
0° - J
j) ϕ = 100°
α
90°- N
80°- M
70°- Gb
60°- J
50°- J
40°- J
30°- J
20°- J
10°- J
0° - J
k) ϕ = 110°
α
90°- N
80°- N
70°- M
60°- L
50°- Gb
40°- J
30°- J
20°- J
10°- J
0° - J
l) ϕ = 120°
α
90°- N
80°- N
70°- N
60°- M
50°- L
40°- L
30°- Gb
20°- J
10°- J
0° - J
m) ϕ = 130°
α
90°- N
80°- N
70°- N
60°- N
50°- M
40°- L
30°- L
20°- L
10°- Gb
0° - J
n) ϕ = 140°
α
90°- N
80°- N
70°- N
60°- N
50°- N
40°- M
30°- L
20°- L
10°- L
0° - L
o) ϕ = 150°
α
90°- N
80°- N
70°- N
60°- N
50°- N
40°- N
30°- L
20°- L
10°- L
0° - L
p) ϕ = 160°
α
90°- Q
80°- Q
70°- Q
60°- Q
50°- Q
40°- P
30°- O
20°- O
10°- O
0° - O
q) ϕ = 170°
α
90°- Q
80°- Q
70°- Q
60°- Q
50°- P
40°- O
30°- O
20°- O
10°- O
0° - O
0.5
0
-0.5
u_j
CE
central marker line
CE
co-rotating CE
ISA
non-rotating CE
counter-rotating CE

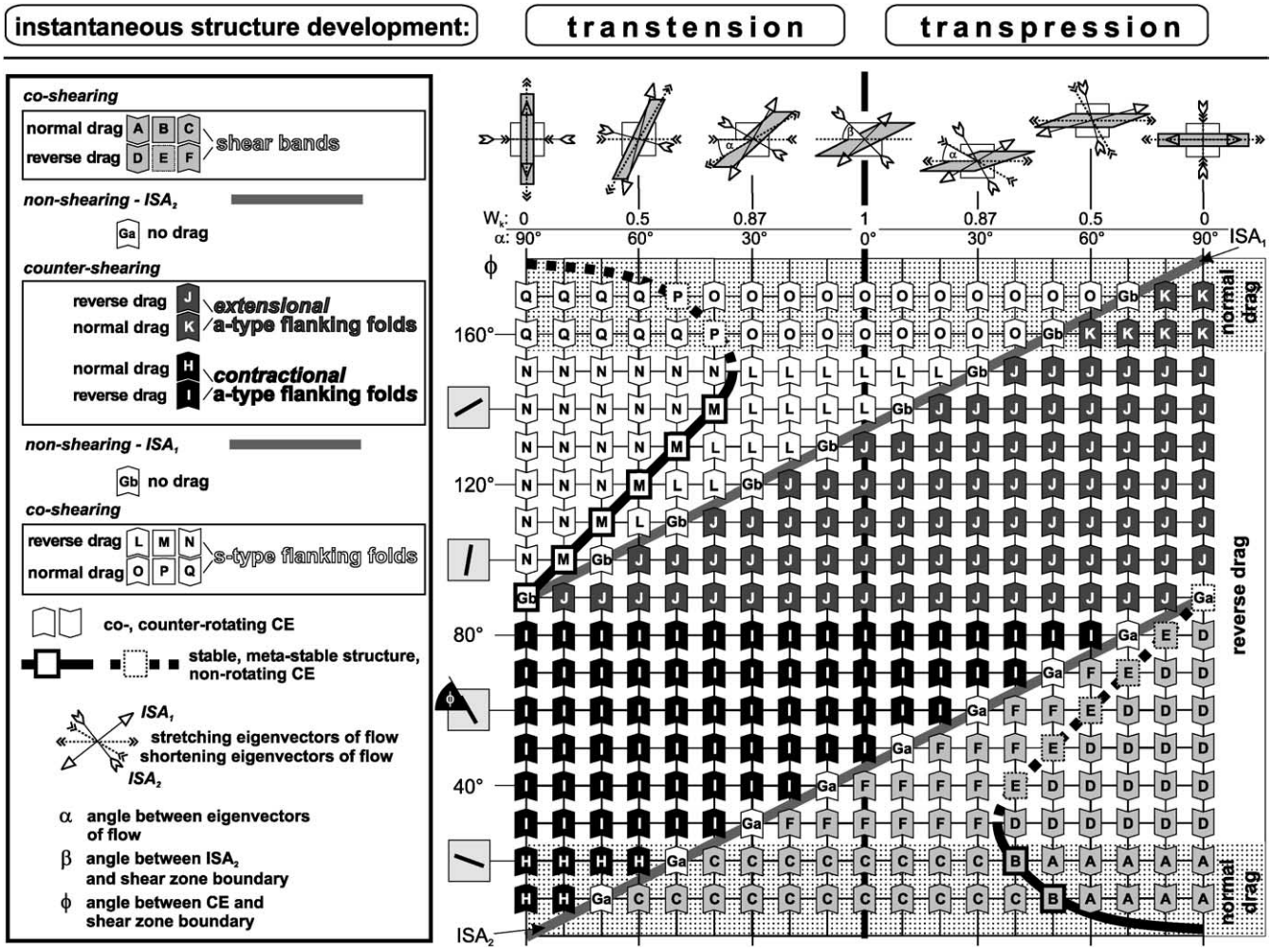

Fig. 4. Diagram illustrating the instantaneous development of flanking structures in transtension and transpression as a function of the flow type (horizontal axis) and the initial orientation of the CE (vertical axis), based on the modelling results in Fig. 3 and Grasemann et al. (2003). Each field with a letter code represents an individual initial starting condition for the numerical simulation. See text for details.

from the non-rotating orientation will result in a progressive, irreversible, either co- or counter-rotation of the CE. This is the case where arrowheads point in opposing directions away from the metastable structure. Accordingly, in transtension, s-type flanking folds are the only structures that have the ability to form stable orientations. They can become (or remain) non-rotating for orientations of $\phi = 90$–$150°$ and are metastable if $\phi = 150$–$180°$. In transpression, shear bands will be the only structures that can form stable orientations. Strictly speaking, structures Ga and Gb on the very left and right pure shear lines do not represent flanking structures as they are non-shearing. Structure Ga, however, forms a metastable structure that can either co-rotate during progressive deformation to develop an a-type flanking fold or counter-rotate into a reverse drag shear band. Gb on the pure shear transtension side will not rotate at all and will keep a stable position without a change in orientation.

Although only thick black lines in the graph in Fig. 4 represent orientations where the rotation velocity is exactly zero, our modelling shows that for orientations deviating in a range of $\sim$10–20° in both directions (α and ϕ), rotation velocities become negligibly small. Consequently in nature, even in very high strain shear zones, structures within this range of orientation will most likely be preserved and can be thought of as being stable. Fig. 5 is an alternative and more concise representation of Fig. 4, where the four general geometrical types of flanking structures with their corresponding mirror images are emphasized in eight different fields.

4. Modelling applications and comparison with natural examples

Grasemann and Stüwe (2001) and Grasemann et al. (2003) noted that the misinterpretation of a-type flanking folds as shear bands lead to the wrong interpretation of the overall sense of shear. According to their model, s-type

flanking folds are, like thrusts, reliable kinematic indicators. However, the broadening of their modelling to a transtensional setting in this work reveals that not only shear bands but also s-type flanking folds are not infallible shear sense indicators, as they can be confused with contractional a-type flanking folds. Especially in transtension, both contractional a- and s-type flanking folds can develop across a large geometrical range. The following two natural examples are discussed in detail in order to illustrate the practical problem of conflicting shear sense resulting from misinterpretation of contractional a- and s-type flanking folds.

4.1. Contractional a-type flanking folds

Fig. 6a shows a plan view of a contractional flanking structure within a major strike-slip zone, which could be interpreted in two ways; either as a dextral s-type flanking fold or a sinistral contractional a-type flanking fold (see Figs. 1 and 5). As the overall movement is known to be left-lateral from boudinaged quartz veins and sigmoidal quartz clasts elsewhere in the outcrop (Passchier et al., 2002), the structure can be identified as a contractional a-type flanking fold. The natural example is in perfect accordance with the modelled structure (Fig. 6b) and shows several characteristics: the displacement along the fault decreases away from point (C), in both directions, downsection and upsection (layers b, c and e) to become zero at the fault tip (T). Note that only for the central marker layer (d) is the drag in the footwall symmetric to the drag in the hanging wall. With increasing distance away from (C), the drag between layers in the footwall and hanging wall becomes more and more asymmetric towards the fault tip (layers b, c and e). The asymmetry can be expressed by the relationship of the layer parallel distance in the footwall (d_f) and the hanging wall (d_h), along which the layer is influenced by a drag along the fault (Fig. 6c). As a general rule for contractional flanking structures, the distance that is larger (either d_f or d_h) always points towards the fault tip (T) in the direction of shear, whereas the shorter distance always points towards the centre of the fault (C). Therefore, in cases where only parts of the fault are exposed or the correlation of offset layers is difficult, this general rule can help to locate the relative position along the fault and extrapolate the entire geometry of the structure.

Fig. 6d shows one possible numerically modelled evolution for the natural example (Fig. 6a), which is dominated by transtensional simple shear flow ($W_k=0.98$). The structure starts to develop at an initial fault angle $\phi=40°$ (stage 1) and co-rotates 14° to its final orientation of $\phi=54°$ (stage 2), developing a contractional a-type flanking fold. If deformation proceeds, the fault will further co-rotate to develop an extensional a-type flanking fold (stage 3).

Note that although the modelled structure dominated by simple shear perfectly coincides with the observed one, the structure could develop the same geometry with a greater pure shear component. For example, the same finite structure could be reproduced under extensional pure shear ($W_k=0$) with less fault rotation (initial $\phi=50°$). Therefore we see that one single structure is not indicative of the flow type. Also note that instead of the modelled slip where the shear stress is zero, some shear stress along the fault will reduce the drag effect (Reches and Eidelman, 1995; Grasemann and Stüwe, 2001). Consequently, as the friction along the fault at the time of formation is unknown, a direct deduction of the kinematic vorticity is not possible.

4.2. s-type flanking folds

Fig. 7a shows a vertical outcrop section from a SW-directed fold and thrust belt in the structurally higher portion of the Himalayas (NW-India) and highlights an example in which a fault-related fold develops with pronounced and symmetric hanging wall and footwall deformation. Fault displacement distance relationships (Williams and Chapman, 1983; Hedlund, 1997) reveal that the displacement not only decreases towards the upper fault tip (T) to become zero, but also shows the same characteristics in the opposite direction, downsection. Consequently, the maximum displacement occurs in the central part of the fault, a feature also described for outcrop scale fault-cored folds from McConnell et al. (1997). The progressive development of the structure (Fig. 7c) has been modelled in general shear transtension ($W_k=0.87$), with an initial fault angle of $\phi=40°$ (stage 1). As the fault co-rotates towards a higher angle $\phi=145°$ (stage 2), an s-type flanking fold starts to develop. After ongoing slip along the fault and further rotation, the folds reveal both a pronounced footwall syncline and hanging wall anticline (stage 3). Despite the good consistency between the natural and modelled structures, the fold shape and displacement distance relationships are relatively insensitive to W_k and a similar final geometry can be obtained across a broad range of W_k depending on the initial orientation and amount of rotation of the fault (CE). Although we are confident that the structure shown in Fig. 7a represents an s-type flanking fold because the SW-directed transport in the section is well established in detail (Wiesmayr and Grasemann, 2002), the structure could, in contrast, reveal a contractional a-type flanking fold with the opposite shear sense. Hence, the correct interpretation of a single structure without additional kinematic information is problematic and is discussed in the following section.

4.3. Determination of flanking structures for the use as shear sense indicators

In nature, the four general geometrical types of flanking structures (Fig. 1) can be easily identified using the following criteria: (1) whether the offset along the CE is contractional or extensional and (2) whether the bending of the HE (i.e. the drag) is convex or concave in the direction of shear. However, the determination of an individual

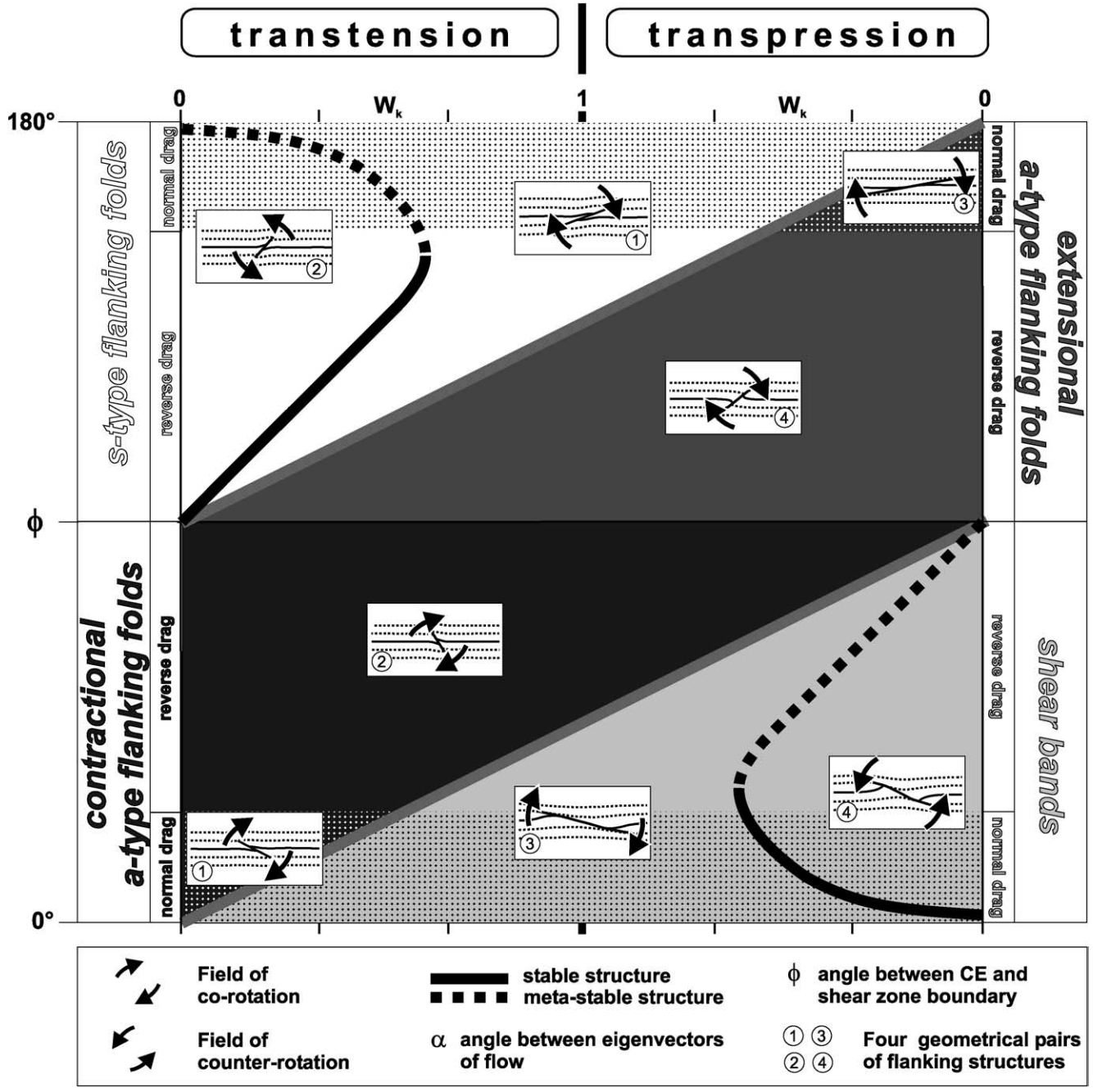

Fig. 5. Alternative presentation to Fig. 4 for the instantaneous development of flanking structures, where the four general geometrical types with their corresponding mirror images are emphasized.

structure without additional knowledge of the bulk shear sense is not reliable. As a consequence, the shear sense from a single structure alone is ambiguous, as theoretically a corresponding mirror image always exists (Figs. 1 and 5). Nevertheless, if more than one flanking structure is developed together, they may be used to uniquely identify the structures and to determine the bulk shear sense. Such an application is shown in Fig. 8, where finite structures are plotted in the diagram for instantaneous structural development. Fig. 8a and c depicts differently annotated identical photographs showing two flanking structures side by side that are developed within metamorphic layers of a marble mylonite from the Naxos metamorphic core complex (Greece). If a dextral shear sense is assumed (Fig. 8a), the two structures have angles $\phi = 80°$ and 125° between the CE and the shear zone boundary and they therefore have to be interpreted as a contractional reverse drag a-type flanking fold and an extensional reverse drag a-type flanking fold, respectively. If we assume that the structures in Fig. 8 record low strain and therefore only a rotation of a few degrees, the

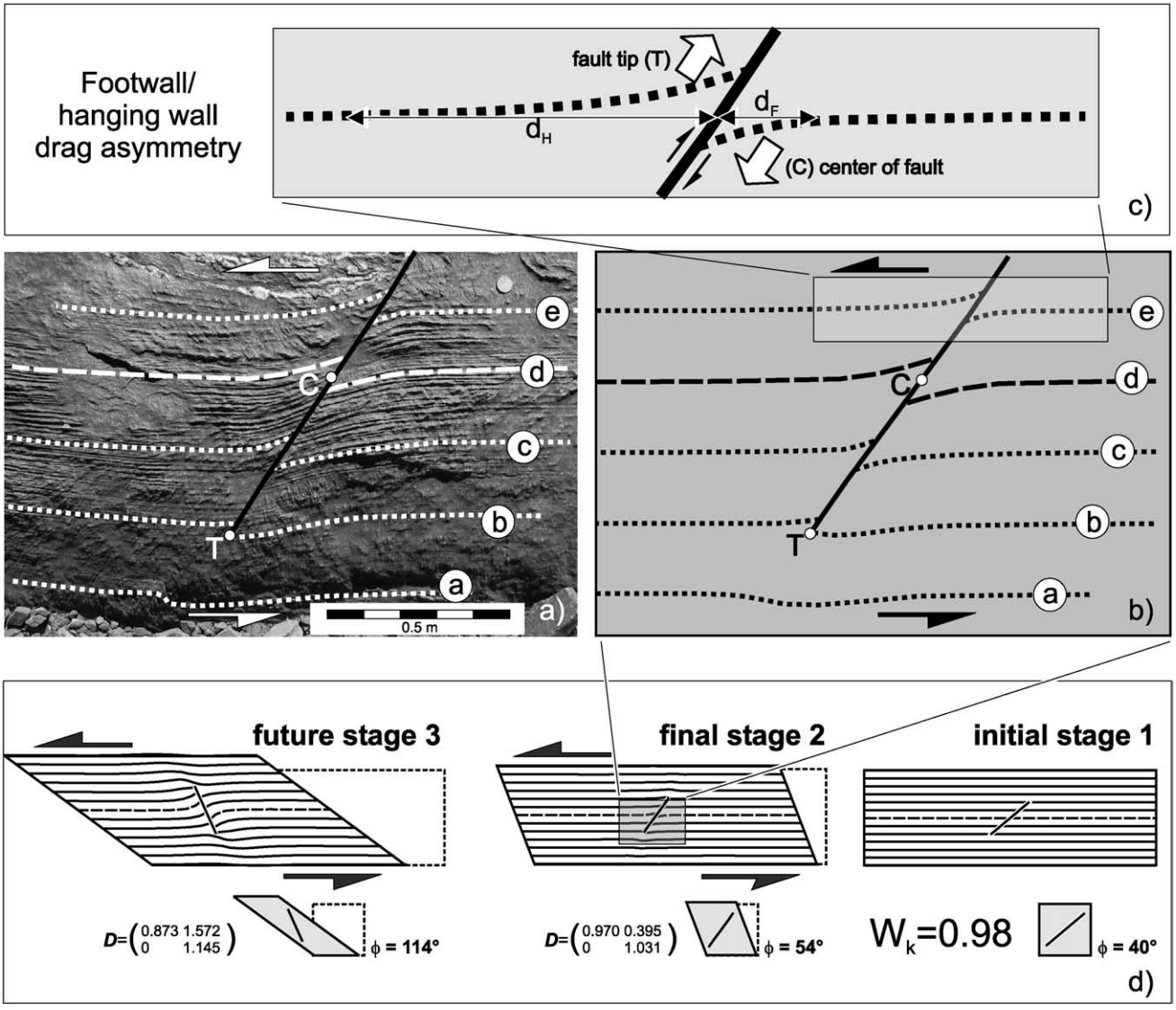

Fig. 6. Characteristics of contractional a-type flanking folds. (a) Natural example from major NE–SW-trending left lateral strike slip zone in Namibia [S20°40′33.0″ E14°25′49.8″] C—centre of the fault, T—fault tip, a—layer not affected by faulting, b, c, e—layers affected by faulting, creating asymmetric drag in the footwall with respect to the hanging wall, d—central marker layer, where displacement is largest and drag in the footwall is symmetric to drag in the hanging wall. (b) Corresponding structure obtained by mechanical modelling. (c) Close-up of (b) showing asymmetric drag between footwall and hanging wall from which the T and C can be inferred. (d) Progressive flanking fold evolution where for each stage the fault angle ϕ is shown. For stages 2 and 3 the corresponding deformation gradient tensor **D** is given.

contractional a-type flanking fold probably formed at an angle of $\phi \sim 70°$. They can therefore only coexist within a flow type between $\alpha = 24°$ (transtension) and $\alpha = 52°$ (transpression), where these structures will plot together as points on a vertical line of constant vorticity (Fig. 8b). Alternatively if a sinistral shear sense is assumed (Fig. 8c), the two structures have to be interpreted as a reverse drag s-type flanking fold and a reverse drag shear band, with finite angles $\phi = 100°$ and 55°, respectively. However, under the same argument of constant vorticity, these structures can never plot as points along a common vertical line (Fig. 8b) as reverse drag shear bands cannot develop under the flow conditions where s-type flanking folds with a specific orientation of $\phi = 100°$ form. Consequently, a sinistral interpretation of the mylonitic shear zone can be excluded, and this is consistent with abundant independent shear sense criteria that exist for the region from other studies (Structural Processes Group, work in progress).

However, note that although in this example the structures can be used for the determination of the shear sense (dextral), they can still form under a broad range of W_k from simple shear dominated transtension ($W_k = 0.9$; $\alpha = 24°$) to general shear transpression ($W_k = 0.6$; $\alpha = 52°$). Other coexisting flanking structures (e.g. normal drag shear

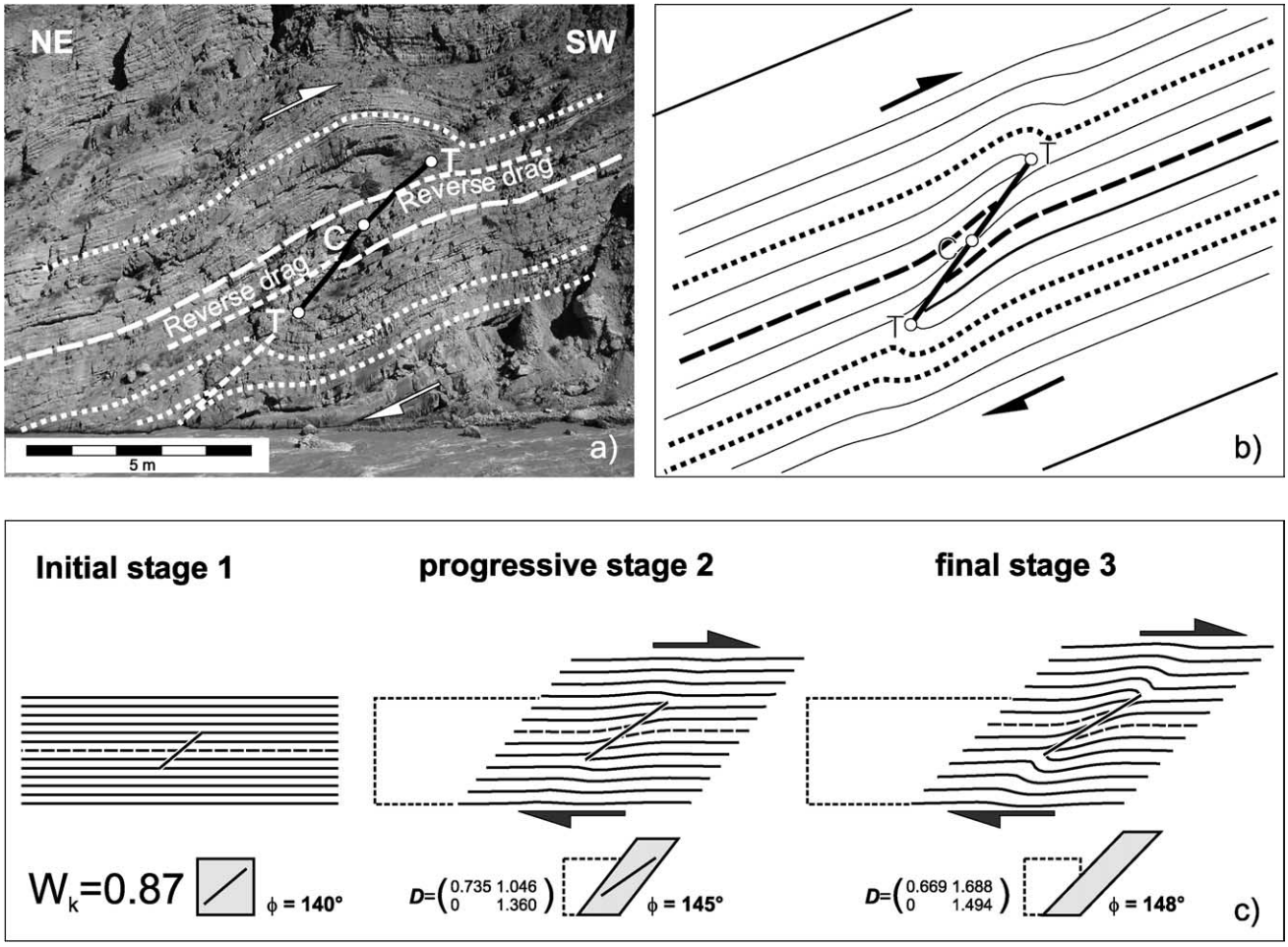

Fig. 7. (a) Superb example of an s-type flanking fold formed within Jurrassic Limestones in the Pin Valley in Spiti, N-India (N32°05′34, 67″, E78°09′20, 38″). Looking SE. C—centre of the fault, T—fault tip. (b) Corresponding structure obtained by mechanical modelling. (c) Progressive flanking fold evolution where for each stage the fault angle ϕ is shown. For stages 2 and 3 the corresponding deformation gradient tensor **D** is given (courtesy of Mario Habermüller and Klaus Arnberger).

bands and extensional normal drag a-type flanking folds or normal drag shear bands and high angle reverse drag s-type flanking folds) would indicate a much narrower range for pure shear transpression and transtension, respectively, and could therefore not only be used as shear sense, but also flow-type indicators.

5. Discussion

5.1. Fault drag

Normal drag along faults is a well established and described phenomenon and has even been used as a shear sense criterion in structural geology textbooks (e.g. Hills, 1963; Billings, 1972; Twiss and Moores, 1992). The generally accepted intuitive explanation is that normal fault drag formed by a reduction in the flow velocity of the wall rocks by the frictional resistance along the fault. Observations of reverse drag or gradual change from normal to reverse drag along faults question this interpretation, however. Hamblin (1965) suggested a model in which normal movement along a listric fault results in an additional volume in the hanging wall in which the rocks collapse, thereby forming reverse fault drag. This explanation is still generally accepted (Tearpock and Bischke, 2003, and references cited therein).

This study and published mechanical models (Grasemann et al., 2003) that examine perfectly frictionless faults without volume change both predict geometries that completely match natural structures and we are implying that the above explanations cannot be accepted as a general rule for the formation of normal and reverse drag structures associated with faults. As an alternative, we conclude with Barnett et al. (1987) and Reches and Eidelman (1995) that most of the observed drag effects are the result of flow perturbation within the host rocks induced by motion along the fault. Interestingly, Grasemann et al. (2003) showed

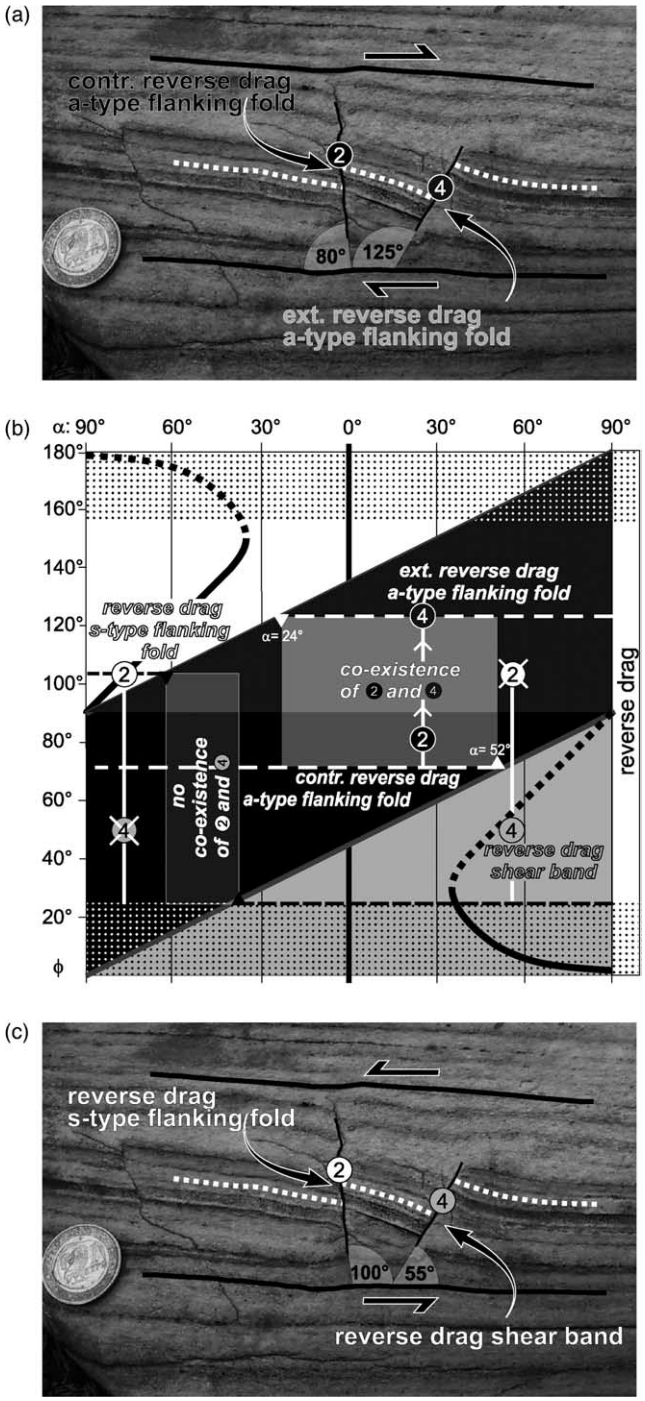

Fig. 8. Application of the diagram of instantaneous development of flanking structures for the determination of the bulk shear sense. The identification of flanking structures within a marble mylonite from Naxos (Greece) [N37°11′26, 2″, E25°30′48, 8″] depends on the inferred shear sense. (a) Dextral interpretation. (b) Diagram of instantaneous development of flanking structures with structures from (a) and (c) plotted as points (structures are labelled after the four general geometrical types of flanking structures; see Fig. 1). (c) Sinistral interpretation.

with their model results that normal drag will form completely insensitive to the kinematic vorticity number of the bulk flow at low angles ($<25°$) between the shear zone boundary and a fault, dipping either with or against the shear direction. This observation is probably confirmed by natural examples (Passchier, 1984), although detailed investigations are still lacking.

The present work confirms the model results of Grasemann et al. (2003) and extends their observations to transtensional shear zones where, similarly, the fault drags of the central marker lines are only normal if the marker lines meet the fault at low angles; otherwise fault drag is always reverse.

5.2. Flanking structure development as flow type indicators (transpression vs. transtension)

The extension of our modelling for plane strain transtension predicts that all three types of flanking structures can develop instantaneously, but with different probability. In transtension, the likeliness of shear band development decreases from simple shear to become zero at the pure shear transtension end member. It is rather unlikely that shear bands will be preserved in natural widening shear zones, as the CE will immediately co-rotate towards higher fault angles and will be reactivated to form contractional a-type flanking folds (Figs. 4 and 5). Accordingly, a- and s-type flanking folds are the preferred structures forming within a large geometrical range in transtension. Grasemann et al. (2003) have shown that shear bands are the only stable structures in transpression (structures B in our Fig. 4), and will therefore most likely be preserved in transpressional shear zones. In contrast to that, s-type flanking folds form the only stable structures in transtension at angles $\phi = 90$–$155°$ as a function of the kinematic vorticity and are represented by thick bold lines in Figs. 4 and 5 (structures B and M in Fig. 4). Note that flanking structures in the vicinity of the line of stable structures (ϕ, $\alpha \pm 10$–$20°$) are also very likely to be preserved in natural shear zones and can be referred to as stable as the rotation rates are still very small with respect to high effective shear strains. Although we are aware that we only modelled low strain structures, up to $\gamma = 2$–3, the same flanking structure geometries are obtained for high strains (e.g. Exner et al., 2004; Kocher and Manckte-low, 2004), where one could expect structures like foliation boudinage to develop. As a consequence, a conspicuously frequent occurrence and preservation of s-type flanking folds would be indicative of transtension (i.e. layer parallel shortening and shear zone thickening normal to the shear zone boundaries). Note, however, that at even larger shear strains ($\gamma \sim 5$–7) s-type flanking folds will start to become unrecognisable (Exner et al., 2004).

5.3. Comparison with existing fault related fold models

Plane strain transtensional flow strongly resembles the

tectonic boundary conditions in compressional fold and thrust belts, where there is a shortening parallel to and thickening normal to a basal detachment probably including a non-coaxial component due to back-shear. Our natural examples show that flanking structures develop at different scales, from the outcrop scale within ductile shear zones up to mesoscopic scale faults in fold and thrust belts (Figs. 6–8). Several classic kinematic and mechanical models for fault-related folds have been established, which either explain the development of hanging wall anticlines, like *fault bend folding* (Suppe, 1983; Salvini et al., 2001) and *fault-propagation folding* (Suppe, 1985; Suppe and Medwedeff, 1990) or explain both; the development of *footwall synclines* and *hanging wall anticlines*, like *trishear fault-propagation folding* and *forced folding* (Erslev, 1991; Allmendinger, 1998; Johnson and Johnson, 2002) or *break-thrust folding* (Fischer et al., 1992; Woodward, 1997) or a combination of *trishear fault-propagation folding* and *break thrust folding* (Erslev and Mayborn, 1997).

The fundamental difference between our model for the development of flanking structures and those mentioned above is that we incorporate the following three characteristics: (1) the fault does not necessarily maintain a stable orientation, but can either co- or counter-rotate during progressive development. (2) The displacement along the fault has its maximum in the centre of the fault and decreases with the same ratio downsection as it increases upsection towards the fault tip as is shown by McConnell et al. (1997) for several outcrop scale natural examples. Because the fault in this case does not continue into a bedding parallel detachment to join an upper and/or lower flat, the fault displacement–distance relationships will be fundamentally different. (3) The tip of the fault remains stationary, while displacement continues, as is the case for tip-line folds (Williams and Chapman, 1983) and fault displacement gradient folds (Wickham, 1995), which Thorbjornsen and Dunne (1997) call *fault arrest folds*.

Other models, which closely resemble the natural example of Fig. 7 with symmetrical hanging wall and footwall deformation, are those of (1) *relay zones* between segmented thrust faults (Nicol et al., 2002) and (2) *symmetrical limb wedge thrusts*, where fault-bend folds form in both the hanging wall and the footwall (Mitra, 2002). However, there are differences between these models and ours. Relay zones necessarily need two faults to form, while flanking folds form along a single fault. In contrast to symmetrical limb wedge thrusts, where the fault passes into layer-parallel detachments, firstly the fault in flanking folds is pinned, and secondly, layers form a footwall and hanging wall cut-off and exhibit reverse drag in the vicinity of the fault tip (Fig. 7) instead of continuing fault-parallel (for at least half the distance of the maximum displacement), as is characteristic for fault-bend folding. Another difference of our model to that of many other fault-related fold models where layering plays a key role is that here layering behaves in a purely passive manner.

Our modelling boundary conditions cover the entire range from simple shear over general shear to the pure shear end member and it is straightforward to compare flanking structures with existing fault-related fold models and tectonic settings that have similar boundary conditions, and to deduce the differences and consequences that arise for cross-section interpretation. For example, boundary conditions for fault-bend folds with fault-parallel flow (Egan et al., 1999), which mostly require additional back shear at the trailing edge and a flexural slip mechanism, resemble those of simple shear dominated s-type flanking folds. Fault propagation fold models that require layer-parallel shortening and layer-normal thickening by penetrative strain (e.g. Mitra, 1990) can be compared with pure shear dominated end members of s-type flanking folds.

From the features discussed above, fundamental consequences for balancing and restoration techniques arise from three salient observations: (1) the fault related to folding does not join a layer-parallel or common detachment (e.g. fig. 3 in Mitra, 1990); a situation for which no alternative balanced model exists up to now. (2) Faults may rotate during progressive deformation, a fact that is considered in none of the established restoration procedures; restored fault trajectories will look markedly different if this phenomenon is taken into account. (3) Flanking structure development accompanies footwall deformation and must be considered in the restoration procedure, as already critically commented by Ramsay (1992); footwall deformation might have been underestimated or simplified in many fault related fold models and is much more common than literature has previously suggested.

6. Conclusions

The broadening of the regime of flanking structure development to include transtension (i.e. layer parallel shortening and layer normal thickening) from pure shear to the simple shear end member reveals that four general geometrical types of flanking structures exist, and that these can be distinguished by (1) the extensional or contractional offset and (2) the normal or reverse drag of the central marker layer.

For each of these four general types, a corresponding mirror image with the opposite sense of shear along the fault (CE) exists, bestowing an ambiguity even for thrusting kinematics, when flanking structures are used as shear sense indicators. If at least one additional flanking structure that developed at a separate stage of progressive deformation is preserved, it is in many cases possible to deduce the overall shear sense and, under favourable conditions, to estimate the flow type.

While shear bands are indicative of transpressional tectonic settings, development and preservation of shear bands in transtension is limited. Flanking folds of a- and

s-type are the preferred structures forming within a large geometrical range in transtension. S-type flanking folds represent the only stable structures in transtension at fault angles $\phi = 90$–$155°$, depending on the kinematic vorticity.

Flanking structures develop at different scales, from microscopic to outcrop, within ductile shear zones up to mesoscopic or probably even macroscopic faults in fold and thrust belts. Flanking folds therefore (and especially s-type flanking folds) have to be considered as a new important addition to existing fault-related fold models (i.e. fault-bend folds, fault-propagation folds, detachment folds and break-thrust folds).

The fundamental differences of our model to existing fault-related fold models are: (1) the fault does not necessarily maintain a stable orientation but may rotate during progressive development; (2) the drag can change from reverse to normal along the fault; and (3) the displacement along the fault has its maximum in the centre of the fault and decreases to zero in both directions, downsection and upsection towards fixed fault tips, in contrast to fault propagation folds, where it only decreases upward or remains constant in break-thrust folds. Flanking structures are not associated with, and do not require, ramp flat geometries, as in fault-bend folds or fault-propagation folds.

As flanking structures always cause footwall deformation, they provide an attractive explanation for the development of joined footwall synclines and hanging wall anticlines and should therefore be considered and re-investigated in the cross-section restoration procedures and structural interpretations, as we believe that footwall deformation has been underestimated and simplified in many fault-related fold models.

Acknowledgements

We thank G. Houseman for originally developing the code and T. Barr and L. Evans for their helpful assistance with BASIL. We thank N. Mancktelow, C. Passchier, U. Exner, T. Kocher, H. Rice and E. Draganits for many fruitful discussions about flanking folds. A special "thank you" goes to Klaus Arnberger and Mario Habermüller for providing a picture of their spectacular observation of s-type flanking folds in the Pin Valley shown in Fig. 7a. Thanks to Mike Edwards for critical comments on earlier versions of the manuscript. We acknowledge support from the Austrian "Fonds zur Förderung der wissenschaftlichen Forschung" (FWF grant P-15668-GEO). We thank the editor Richard Norris, and Simon Wallis and Peter Hudleston for their careful and constructive reviews.

References

Allmendinger, R.W., 1998. Inverse and forward numerical modeling of trishear fault-propagation folds. Tectonics 17, 614–656.

Barnett, J.A.M., Mortimer, J., Rippon, J.H., Walsh, J.J., Watterson, J., 1987. Displacement geometry in the volume containing a single normal fault. The American Association of Petroleum Geologist Bulletin 71, 925–937.

Barr, T.D., Houseman, G.A., 1992. Distribution of deformation around a fault in a non-linear ductile medium. Geophysical Research Letters 19, 1145–1148.

Barr, T.D., Houseman, G.A., 1996. Deformation fields around a fault embedded in a non-linear ductile medium. Geophysical Journal International 125, 473–490.

Billings, M.P., 1972. Structural Geology. Prentice-Hall, Englewood Cliffs, NJ.

Egan, S.S., Kane, S., Buddin, T.S., Williams, G.D., Hodgetts, D., 1999. Computer modelling visualisation of the structural deformation caused by movement along geological faults. Computers & Geosciences 25, 283–297.

Erslev, E.A., 1991. Trishear fault-propagation folding. Geology 19, 617–620.

Erslev, E.A., Mayborn, K.R., 1997. Multiple geometries and modes of fault-propagation folding in the Canadian thrust belt. Journal of Structural Geology 19, 321–335.

Exner, U., Mancktelow, N.S., Grasemann, B., 2004. Progressive development of s-type flanking folds in simple shear. Journal of Structural Geology, 26, 2191–2201.

Fischer, M.P., Woodward, N.B., Mitchell, M.M., 1992. The kinematics of break-thrust folds. Journal of Structural Geology 14, 451–460.

Fossen, H., Tikoff, B., 1993. The deformation matrix for simultaneous simple shearing, pure shearing and volume change, and its application to transpression–transtension tectonics. Journal of Structural Geology 15, 413–422.

Fossen, H., Tikoff, B., 1998. Extended models of transpression and transtension, and application to tectonic settings, in: Jones, R.R., Holdsworth, R.E. (Eds.), Continental Transpressional and Transtensional Tectonics Geological Society Special Publication, 135, pp. 15–33.

Grasemann, B., Stüwe, K., 2001. The development of flanking folds during simple shear and their use as kinematic indicators. Journal of Structural Geology 23, 715–724.

Grasemann, B., Fritz, H., Vannay, J.C., 1999. Quantitative kinematic flow analysis from the Main Central Thrust Zone (NW-Himalaya, India): implications for a decelerating strain path and the extrusion of orogenic wedges. Journal of Structural Geology 21, 837–853.

Grasemann, B., Stüwe, K., Vannay, J.C., 2003. Sense and non-sense of shear in flanking structures. Journal of Structural Geology 25, 19–34.

Hamblin, W.K., 1965. Origin of 'reverse drag' on the down-thrown side of normal faults. Geological Society of America Bulletin 76, 1145–1164.

Hedlund, C.A., 1997. Fault-propagation, ductile strain, and displacement–distance relationships. Journal of Structural Geology 19, 249–256.

Hills, E.S., 1963. Elements of Structural Geology. Methuen and Co., London.

Johnson, K.M., Johnson, A.M., 2002. Mechanical analysis of the geometry of forced-folds. Journal of Structural Geology 24, 401–410.

Kocher, T., Mancktelow, N.S., 2004. Numerical modelling of progressive evolution of flanking structure. Bollettino di Geofisica Teorica ed Applicata 45, 304.

Marrett, R., Peacock, D.C.P., 1999. Strain and stress. Journal of Structural Geology 21, 1057–1063.

McConnell, D.A., Kattenhorn, S.A., Benner, L.M., 1997. Distribution of fault slip in outcrop-scale fault-related folds, Appalachian Mountains. Journal of Structural Geology 19, 257–267.

Mitra, G., 2002. Fold-accommodation faults. AAPG Bulletin 86, 671–693.

Mitra, S., 1990. Fault-propagation folds: geometry, kinematic evolution and hydrocarbon traps. AAPG Bulletin 74, 921–945.

Nicol, A., Gillespie, P.A., Childs, C., Walsh, J.J., 2002. Relay zones between mesoscopic thrust faults in layered sedimentary sequences. Journal of Structural Geology 24, 709–727.

Passchier, C.W., 1984. The generation of ductile and brittle shear bands in a low angle mylonite zone. Journal of Structural Geology 6, 273–281.

Passchier, C.W., 1987. Efficient use of the velocity gradient tensor in flow modelling. Tectonophysics 136, 159–163.

Passchier, C.W., 2001. Flanking structures. Journal of Structural Geology 23, 951–962.

Passchier, C.W., Trouw, R.A.J., Ribeiro, A., Paciullo, F.V.P., 2002. Tectonic evolution of the southern Kaoko belt, Namibia. Journal of African Earth Sciences 35, 61–75.

Ramberg, H., 1975. Particle paths, displacement and progressive strain applicable to rocks. Tectonophysics 28, 1–37.

Ramsay, J.R., 1992. Some geometric problems of ramp-flat thrust models. In: McClay, K.R. (Ed.), Thrust Tectonics. Chapman & Hall.

Reches, Z., Eidelman, A., 1995. Drag along faults. Tectonophysics 247, 145–156.

Salvini, F., Storti, F., McClay, K., 2001. Self-determining numerical modeling of compressional fault-bend folding. Geology 29, 839–842.

Suppe, J., 1983. Geometry and kinematics of fault-bend folding. American Journal of Science 283, 684–721.

Suppe, J., 1985. Principles of Structural Geology. Prentice-Hall, Englewood Cliffs, NJ.

Suppe, J., Medwedeff, D.A., 1990. Geometry and kinematics of fault-propagation folding. Eclogae Geologicae Helvetiae 83, 409–454.

Tearpock, D.J., Bischke, R.E., 2003. Applied Subsurface Geological Mapping. Prentice-Hall, Englewood Cliffs, NJ.

Thorbjornsen, K.L., Dunne, W.M., 1997. Origin of a thrust-related fold: geometric vs. kinematic tests. Journal of Structural Geology 19, 303–319.

Twiss, R.J., Moores, E.M., 1992. Structural Geology. W.H. Freeman and Company, New York.

Wickham, J., 1995. Fault displacement-gradient folds and the structure at Lost Hills, California (U.S.A.). Journal of Structural Geology 17, 1293–1302.

Wiesmayr, G., Grasemann, B., 2002. Eohimalayan fold and thrust belt: implications for the geodynamic evolution of the NW-Himalaya (India). Tectonics 21, 8/1–818.

Williams, G., Chapman, T., 1983. Strains developed in the hanging walls of thrusts due to their slip/propagation rate: a dislocation model. Journal of Structural Geology 5, 563–571.

Woodward, N.B., 1997. Low-amplitude evolution of break-thrust folding. Journal of Structural Geology 19, 293–301.